DNA repair protein FANCD2 has both ubiquitination-dependent and ubiquitination-independent functions during germ cell development

Received for publication, September 3, 2022, and in revised form, December 30, 2022 Published, Papers in Press, January 13, 2023,
https://doi.org/10.1016/j.jbc.2023.102905

Simin Zhao[1,2,3,4,5,6,‡], **Chengzi Huang**[1,2,3,4,5,6,‡], **Yajuan Yang**[1,2,3,4,5,6], **Weiwei Xu**[1,2,3,4,5,6], **Yongze Yu**[1,2,3,4,5,6], **Canxin Wen**[1,2,3,4,5,6], **Lili Cao**[1,2,3,4,5,6], **Fei Gao**[1,7], **Yingying Qin**[1,2,3,4,5,6], **Zi-Jiang Chen**[1,2,3,4,5,6,8,9,10], **Ting Guo**[1,2,3,4,5,6,*], and **Shidou Zhao**[1,2,3,4,5,6,*]

From the [1]*Center for Reproductive Medicine, and* [2]*Key Laboratory of Reproductive Endocrinology of Ministry of Education, Shandong University, Jinan, Shandong, China;* [3]*Shandong Key Laboratory of Reproductive Medicine, Jinan, Shandong, China;* [4]*Shandong Provincial Clinical Research Center for Reproductive Health, Jinan, Shandong, China;* [5]*Shandong Technology Innovation Center for Reproductive Health, Jinan, Shandong, China;* [6]*National Research Center for Assisted Reproductive Technology and Reproductive Genetics, and* [7]*Advanced Medical Research Institute, Shandong University, Jinan, Shandong, China;* [8]*Research Unit of Gametogenesis and Health of ART-Offspring, Chinese Academy of Medical Sciences, Jinan, China;* [9]*Shanghai Key Laboratory for Assisted Reproduction and Reproductive Genetics, Shanghai, China;* [10]*Center for Reproductive Medicine, Ren Ji Hospital, School of Medicine, Shanghai Jiao Tong University, Shanghai, China*

Edited by George DeMartino

When DNA interstrand crosslink lesions occur, a core complex of Fanconi anemia proteins promotes the ubiquitination of FANCD2 and FANCI, which recruit downstream factors to repair the lesion. However, FANCD2 maintains genome stability not only through its ubiquitination-dependent but also its ubiquitination-independent functions in various DNA damage response pathways. Increasing evidence suggests that FANCD2 is essential for fertility, but its ubiquitination-dependent and ubiquitination-independent roles during germ cell development are not well characterized. In this study, we analyzed germ cell development in *Fancd2* KO and ubiquitination-deficient mutant (*Fancd2*$^{K559R/K559R}$) mice. We showed that in the embryonic stage, both the ubiquitination-dependent and ubiquitination-independent functions of FANCD2 were required for the expansion of primordial germ cells and establishment of the reproductive reserve by reducing transcription-replication conflicts and thus maintaining genome stability in primordial germ cells. Furthermore, we found that during meiosis in spermatogenesis, FANCD2 promoted chromosome synapsis and regulated crossover formation independently of its ubiquitination, but that both ubiquitinated and nonubiquitinated FANCD2 functioned in programmed double strand break repair. Finally, we revealed that on meiotic XY chromosomes, H3K4me2 accumulation required ubiquitination-independent functionality of FANCD2, while the regulation of H3K9me2 and H3K9me3 depended on FANCD2 ubiquitination. Taken together, our findings suggest that FANCD2 has distinct functions that are both dependent on and independent of its ubiquitination during germ cell development.

Germ cells ensure the perpetuation of genetic information across generations, and they undergo complex processes to develop into mature gametes, including the specification, migration, and proliferation of primordial germ cells (PGCs), sex differentiation, and meiosis (1, 2). The development of germ cells determines the establishment and depletion of the reproductive reserve, and studies into the regulatory mechanisms underlying germ cell development will help to elucidate the pathogenesis of infertility and genetic diseases.

Fanconi anemia (FA) is a rare genetic syndrome characterized by early bone marrow failure, cancer predisposition, congenital malformation, and severe reproductive defects (3). To date, 22 FA genes have been identified in a complex pathway that orchestrates DNA interstrand crosslink (ICL) repair (4, 5). When ICLs occur, the FA core complex (including FANCA, B, C, E, F, G, L, and M) promotes the monoubiquitination of FANCD2 and FANCI. The ubiquitinated FANCD2-FANCI heterodimer then recruits downstream DNA repair factors to complete ICL repair (6). The ubiquitination of human FANCD2 at Lysine-561 is a key step in the activation of the FA pathway, and ubiquitinated FANCD2 forms nuclear foci that represent the sites of DNA repair (7, 8). FANCD2 was recently shown to play a role in transcription-replication conflicts (TRCs) that are generated when the transcriptional apparatus encounters the replication apparatus and cause replication stress and genome instability (9, 10). When TRCs occur, stalled replication forks (RFs) and transcription-associated R-loops activate the FA pathway, and ubiquitinated FANCD2 functions to stabilize RFs and resolve R-loops to overcome TRCs (11–13). These functions requiring the ubiquitination of FANCD2 are considered as ubiquitination-dependent. In addition, FANCD2 can also regulate genome stability when its ubiquitination is not occurred (11), and these roles are referred as independent of ubiquitination and FA pathway activation. For example, the ubiquitination-

‡ These authors contributed equally to this work.
* For correspondence: Shidou Zhao, shidouzhao@sdu.edu.cn; Ting Guo, gtlyp2008@126.com.

independent function of FANCD2 is required for early response to TRCs, which occur when the transiently arrested RNA polymerase II (Pol II) near the promoter region encounters the RFs without forming double strand breaks (DSBs) or ssDNA (12). Under low level of replication stress induced by mitomycin C (MMC) or hydroxyurea, nonubiquitinated FANCD2 protects RFs against nuclease resection and reduces DNA damage (11). In the presence of DSBs induced by etoposide, FANCD2 promotes homologous recombination (HR) independently of its ubiquitination (13). In addition, FANCD2 also promotes the restart of stalled RFs and suppresses the firing of new replication origins independently of its ubiquitination (14). Collectively, these results suggest that FANCD2 maintains genome stability through both ubiquitination-dependent and ubiquitination-independent functions.

FA patients and FA mutant mice are infertile or only rarely fertile (15–19). Our recent study showed that the FA pathway counteracts TRC-induced endogenous replication stress, thus safeguarding genome stability and maintaining the rapid proliferation of PGCs (20). Combined with the findings in FA mutant mice, the drastic reduction in germ cells could be mainly attributed to PGC deficiency during embryonic development (21). However, meiotic defects and epigenetic abnormalities on sex chromosomes during spermatogenesis have also been reported in some FA mutant mice (22–25). These findings emphasize the significant roles of the FA pathway in maintaining germ cell in different stages of development. Compared to the mutant mice without FA core complex components (15, 25, 26), FANCD2-deficient mice displayed more severe germline phenotypes, including a significant reduction of PGCs in the embryonic period, meiotic chromosome synapsis defects, epigenetic modification dysregulation on sex chromosomes during spermatogenesis, and infertility in both female and male mice (27–29). These results suggest that FANCD2 might also function in germ cell development independently of FA pathway activation. Therefore, the ubiquitination-dependent and ubiquitination-independent functions of FANCD2 during gametogenesis need to be further determined.

In this study, we compared *Fancd2*$^{-/-}$ (KO) and the ubiquitination-deficient *Fancd2*$^{K559R/K559R}$ (MT) mice to elucidate the ubiquitination-dependent and ubiquitination-independent functions of FANCD2 during germ cell development. We found that both the genome stability during PGC expansion and the key meiotic events including HR repair and epigenetic modification of sex chromosomes required both the ubiquitination-dependent and ubiquitination-independent functions of FANCD2, thus providing a deeper understanding of the pathogenesis of infertility in FA patients.

Results

The FA pathway is inactive in KO and MT mice

To determine the functions of FANCD2 that are dependent on or independent of its ubiquitination in germ cell development, we generated KO and MT mouse models using the CRISPR/Cas9 technology. For the KO mouse, exons 4 to 16 were deleted, resulting in a premature stop codon at 42 bp downstream of exon 3 (Fig. 1, *A* and *B*). For the MT mouse, p.K559R (AAG to AGG) was introduced (Fig. 1*C*) to generate the ubiquitination-defective FANCD2 MT protein (20).

To confirm the functional defects of FANCD2 in KO and MT mice, Western blotting and immunofluorescence staining were conducted to detect the activation of the FA pathway, which is indicated by FANCD2 ubiquitination and nuclear foci formation. In WT mouse embryonic fibroblasts (MEFs), FANCD2 was slightly ubiquitinated in unperturbed conditions and was significantly ubiquitinated after ICL induction by MMC treatment, whereas FANCD2 was undetectable in KO MEFs and only nonubiquitinated FANCD2 was detected in MT MEFs (Fig. 1*D*). In addition, the immunofluorescence staining showed that FANCD2 was highly expressed in WT PGCs at embryonic day (E) 11.5 and formed a large number of foci in the nuclei of PGCs, but no signals were detected in KO PGCs and FANCD2 was diffusely distributed in the nuclei of MT PGCs (Fig. 1*E*). Taken together, these findings suggest that the FA pathway is inactive in both KO and MT mice.

Both KO and MT embryos show significant loss of PGCs

A general characteristic of FA-null mice was the profound loss of PGCs during embryonic development (21). In order to distinguish the functions of ubiquitinated and nonubiquitinated FANCD2 in germ cell development, embryos at various stages were collected to examine the number of germ cells. Alkaline phosphatase staining showed that the distribution pattern of PGCs in WT, KO, and MT embryos was similar at E8.5, E9.5, and E11.5 (Fig. 2*A*), indicating the relatively normal migration of PGCs. The numbers of PGCs in WT, KO, and MT embryos were comparable at E8.5 (Fig. 2, *A* and *B*), indicating that the specification of PGCs was not obviously affected in KO and MT embryos. However, at E9.5, the number of PGCs was reduced in both KO and MT embryos, but there was no difference between the two genotypes (Fig. 2, *A* and *B*), implying that only ubiquitinated FANCD2 was required for PGC proliferation before E9.5. PGCs were dramatically decreased in MT embryos compared to WT controls in the E11.5 genital ridges (Fig. 2, *A* and *B*), indicating a key role of ubiquitinated FANCD2 in PGC development. In addition, fewer PGCs were seen in KO embryos than those in MT embryos (Fig. 2, *A* and *B*), suggesting that rapid PGC expansion at E9.5-E11.5 also required the ubiquitination-independent function of FANCD2. Consistent with this, germ cells in both KO and MT gonads were dramatically reduced at E13.5 and E18.5, but more germ cell loss was observed in KO embryos (Fig. 2, *C*–*F*). Taken together, these results suggest that ubiquitinated FANCD2 is essential for PGC development, while nonubiquitinated FANCD2 also plays a role in PGC expansion.

KO and MT PGCs show different increases in TRCs and DNA damage

Actively proliferating PGCs are coupled with global transcriptional upregulation (30, 31). We have recently reported

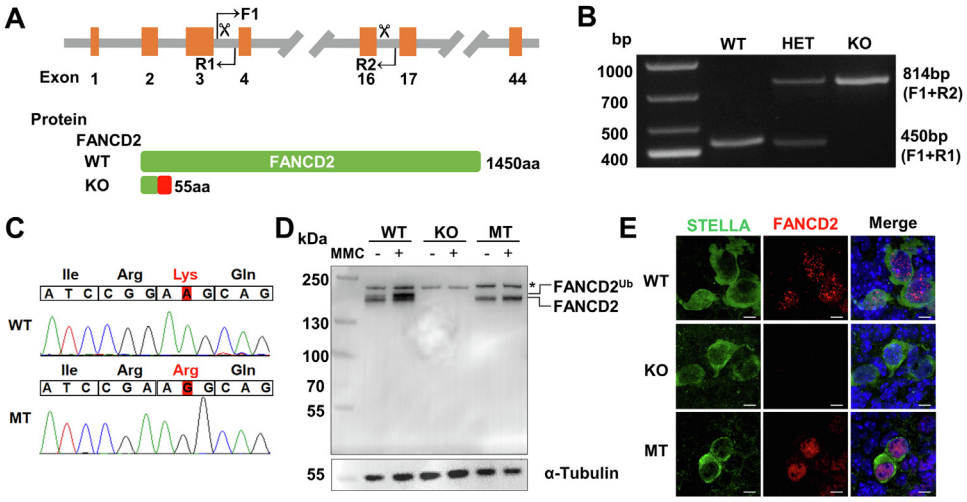

Figure 1. The FA pathway was inactive in KO and MT mice. *A*, schematic diagram of the generation of *Fancd2* KO mice with the location of the targeting gRNA region and the genotyping primers indicated with *scissors* and *black arrows*, respectively. *B*, genotype results determined by PCR in *Fancd2* KO mice. *C*, genotype results for WT and MT mice using Sanger sequencing. *D*, expression of FANCD2 in WT, KO, and MT MEFs treated with 50 ng/ml MMC for 12 h were analyzed by Western blotting with α-Tubulin as the loading control. *E*, immunofluorescence staining for FANCD2 *(red)* and STELLA (*green*) in WT, KO, and MT genital ridges at E11.5. Cell nuclei were counterstained with Hoechst 33342 (*blue*). Scale bars represent 5 μm. KO, *Fancd2*$^{-/-}$; MT, *Fancd2*$^{K559R/K559R}$; FA, fanconi anemia; MEF, mouse embryonic fibroblast; MMC, mitomycin C.

that PGCs are faced with a high frequency of TRCs and the FA pathway counteracts TRC-induced genome instability, thus enabling the rapid proliferation of PGCs (20). To characterize the ubiquitination-dependent and ubiquitination-independent functions of FANCD2 in resolving TRCs in PGCs, a proximity ligation assay (PLA) using antibodies against proliferating cell nuclear antigen (an indicator of the replication machinery) and Pol II (an indicator of the transcriptional machinery) was performed to detect TRCs in WT, KO, and MT PGCs at E11.5. As expected, increased TRCs were observed in MT PGCs compared to WT PGCs (Fig. 3, *A* and *B*), indicating the essential role of ubiquitinated FANCD2 in resolving TRCs. Significantly, we observed a greater increase of PLA foci in KO PGCs than MT PGCs (Fig. 3, *A* and *B*), which implied that the resolution of TRCs in PGCs also required the ubiquitination-independent function of FANCD2. We further evaluated DNA damage by immunofluorescence staining against 53BP1, a marker for DSBs, in WT, KO, and MT genital ridges at E11.5. The proportion of 53BP1-positive PGCs was significantly increased in MT embryos than WT embryos, and a further increased proportion was observed in KO embryos compared to MT embryos (Fig. 3, *C* and *D*), indicating increased DNA damage in MT embryos and more DNA damage in KO than MT embryos. Collectively, both ubiquitinated and non-ubiquitinated FANCD2 function to reduce TRCs and safeguard genome stability in PGCs during expansion.

More germ cells were preserved in MT than KO mice after birth

To further distinguish the ubiquitination-dependent and ubiquitination-independent functions of FANCD2 in germ cell development, detailed histological analyses of gonads were conducted after birth. Compared with WT females, follicles in postnatal day (PD) 3 ovaries from KO and MT females were significantly reduced (Fig. 4*A*). Although more follicles were found in PD3 MT ovaries than in KO ovaries, follicles were completely exhausted in 2-month KO and MT ovaries (Fig. 4, *B* and *C*), suggesting that both KO and MT females suffered premature depletion of oocytes.

Next, we analyzed the influence of FANCD2 dysfunction on males. We found that the testes of KO and MT adult male mice were smaller than those of their WT siblings, and the ratio of testis to body weight in KO and MT mice was significantly lower than that in WT controls (Fig. 5*A*). Histological analyses showed that at PD3 and PD35, more germ cells were present in the seminiferous tubules of MT mice than in those of KO mice (Fig. 5*B*). Because the testes of KO and MT mice displayed a mosaic pattern, we further classified the seminiferous tubules (Fig. 5*D*). In the testes of KO mice, only 18.85% of the seminiferous tubules had relatively normal morphology, 71.14% of the tubules only contained Sertoli cells, 3.48% of the tubules manifested massive germ cell loss, and 6.53% of the tubules had round spermatid as the most advanced developmental stage. In contrast, in the testes of MT mice, 45.74% of the seminiferous tubules had relatively normal morphology, 42.19% of the tubules contained only Sertoli cells, 3.84% of the tubules manifested massive germ cell loss, and 8.23% of the tubules had round spermatids as the most advanced developmental stage (Fig. 5, *C*–*E*). In accordance with the histological results of testis sections, small numbers of sperm were detected in the epididymides of MT mice, but sperm were rarely found in KO epididymides (Fig. 5*C*). Significantly, fertility tests showed that 4 of 6 MT male mice were fertile, while only 1 of 6 KO male mice were fertile (Fig. 5*F*). We supposed that the greater number of PGCs in MT embryos than those in KO embryos was one reason for this difference in fertility. In addition, because FANCD2 has been reported to promote chromosome synapsis and to regulate histone methylation on sex chromosomes during meiosis (28, 29), the distinct ubiquitination-dependent and

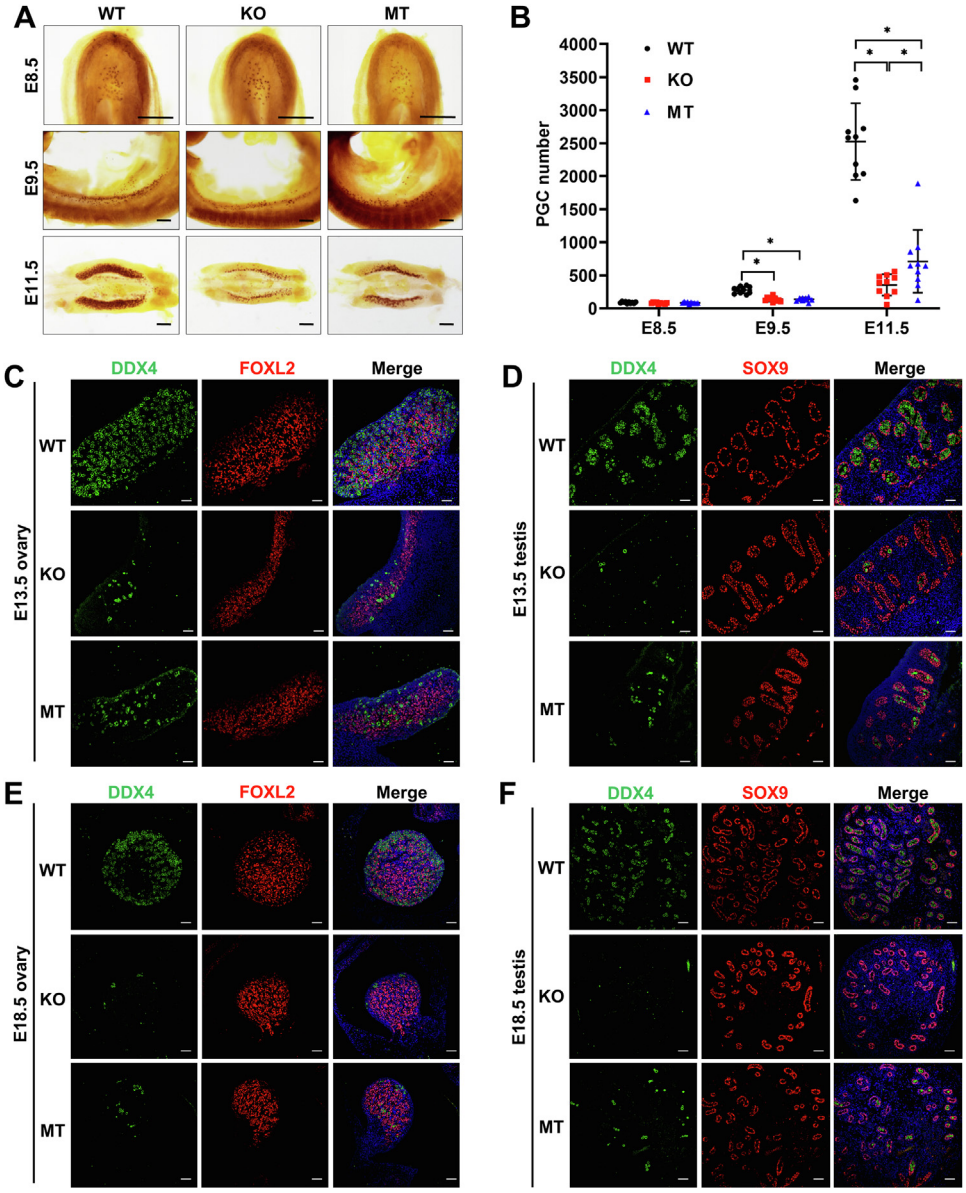

Figure 2. The monoubiquitylation-dependent function of FANCD2 was essential for PGC development. *A*, alkaline phosphatase staining of WT, KO, and MT whole mounts at E8.5 and E9.5, and genital ridges at E11.5. Scale bars represent 200 μm. *B*, counting of PGCs in WT, KO, and MT embryos at E8.5, E9.5, and E11.5. Ten embryos from each embryonic stage were included per genotype. Data are presented as mean ± SD. *$p < 0.05$. Immunofluorescence staining for DDX4 (germ cell marker; *green*) and FOXL2 (pregranulosa marker; *red*) in E13.5 (*C*) and E18.5 (*E*) ovaries from WT, KO, and MT embryos. Cell nuclei were counterstained with Hoechst 33342 (*blue*). Scale bars represent 50 μm. Immunofluorescence staining for DDX4 (*green*) and SOX9 (Sertoli cell marker; *red*) in E13.5 (*D*) and E18.5 (*F*) testes from WT, KO, and MT embryos. Cell nuclei were counterstained with Hoechst 33342 (*blue*). Scale bars represent 50 μm. KO, *Fancd2*$^{-/-}$; MT, *Fancd2*$^{K559R/K559R}$; PGC, primordial germ cell.

ubiquitination-independent functions of FANCD2 during spermatogenesis may be another explanation for the differences in male reproduction.

The meiotic process was more severely impaired in KO spermatocytes

We next analyzed the meiotic progress in the two mouse models. Both KO and MT mice showed relatively normal meiotic progression, as evidenced by the distribution of spermatocytes at various stages of meiotic prophase I (Fig. 6, *A* and *B*). However, we found that the number of pachytene spermatocytes with synapsis defects was increased in KO mice (Fig. 6*C*), while there was no difference between WT and MT mice. These results suggest that FANCD2 promotes homologous chromosome synapsis during meiosis independently of its ubiquitination.

Because of its important roles in DNA damage response (DDR) and HR in mitosis (4, 32, 33), we wondered whether FANCD2 also participates in DSBs' repair during meiosis. We performed immunostaining for phosphorylated H2AX (γH2AX), a marker for DSB repair, on chromosome spreads from WT, KO, and MT spermatocytes. The pattern of γH2AX signals was similar in WT, KO, and MT spermatocytes at leptotene and zygotene stages (Fig. 6*D*). However, in KO and MT mice, 64.29% and 33.36% of the pachytene spermatocytes

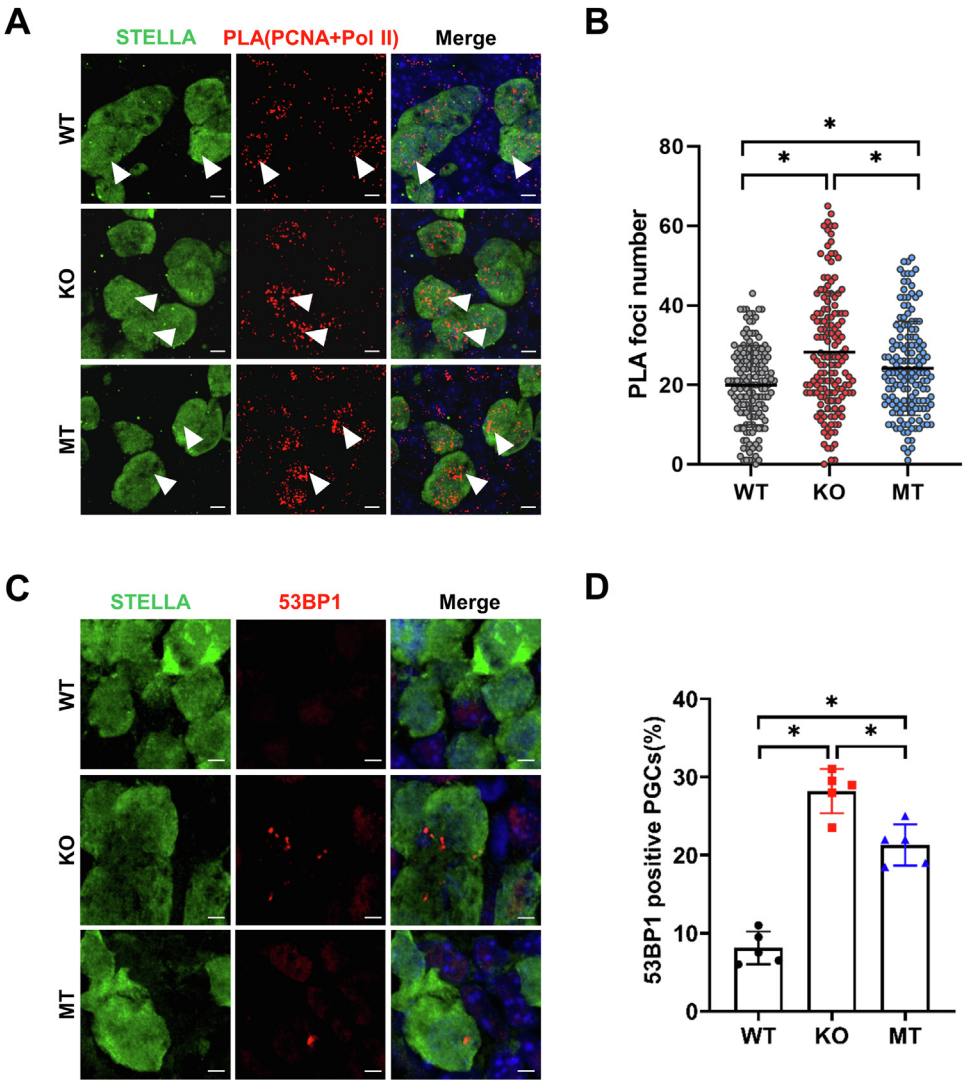

Figure 3. KO and MT PGCs showed increased TRCs and DNA damage. *A*, representative images of PCNA-Pol II PLA foci (*red*) in E11.5 genital ridges from WT, KO, and MT embryos. PGCs were stained with anti-STELLA body (*green*) and Cell nuclei were counterstained with Hoechst 33342 (*blue*). Scale bars represent 5 μm. *Arrowheads* indicate representative PGCs. *B*, numbers of PLA foci per nucleus in PGCs (STELLA-positive cells; *green*) in E11.5 genital ridges from WT, KO, and MT embryos. A total of 150 cells were analyzed per genotype. *C*, immunofluorescence staining for STELLA (*green*) and 53BP1 (*red*) in E11.5 genital ridges from WT, KO, and MT embryos. Cell nuclei were counterstained with Hoechst 33342 (*blue*). Scale bars represent 5 μm. *D*, the proportion of 53BP1-positive PGCs in E11.5 genital ridges from WT, KO, and MT embryos. Five embryos from each genotype were analyzed. Data are presented as mean ± SD. *$p < 0.05$. KO, *Fancd2*$^{-/-}$; MT, *Fancd2*$^{K559R/K559R}$; PGC, primordial germ cell; Pol II, polymerase II; PLA, proximity ligation assay; PCNA, proliferating cell nuclear antigen; TRC, transcription-replication conflict.

showed abnormal γH2AX staining (Fig. 6*F*), respectively, as indicated by γH2AX signals at asynaptic sites in pachytene-like cells or expansion of the γH2AX signals on autosomes (Fig. 6*E*). In contrast, these types of abnormal γH2AX signals were detected in only 13.98% of the WT pachytene spermatocytes (Fig. 6*F*). Collectively, these data suggest that FANCD2 promotes DSB repair in meiotic progression through both ubiquitination-dependent and ubiquitination-independent functions. Furthermore, the meiotic recombination was detected by immunostaining against RAD51, a recombinase in meiotic DSB repair, and comparable numbers of RAD51 foci in leptotene and zygotene spermatocytes were observed in the three genotypes (Fig. 7, *A* and *B*). However, at pachytene stage, consistently with delayed DSB repair in MT and KO spermatocytes, more persistent RAD51 foci were detected in MT than WT spermatocytes, and a further increase of RAD51 foci numbers was observed in KO than MT pachytene spermatocytes (Fig. 7, *A* and *B*), indicating that both ubiquitinated and nonubiquitinated FANCD2 promote meiotic recombination.

Crossover is an important event in meiotic recombination which is essential for the proper segregation of homologous chromosomes (34). To analyze whether crossover formation was influenced in KO and MT spermatocytes, we examined the MLH1 foci in late pachytene spermatocytes. An apparent increase in MLH1 foci numbers was observed in KO spermatocytes, but there was no difference between WT and MT spermatocytes (Fig. 7, *C* and *D*). These results indicate that nonubiquitinated FANCD2 regulates the crossover formation in male meiosis.

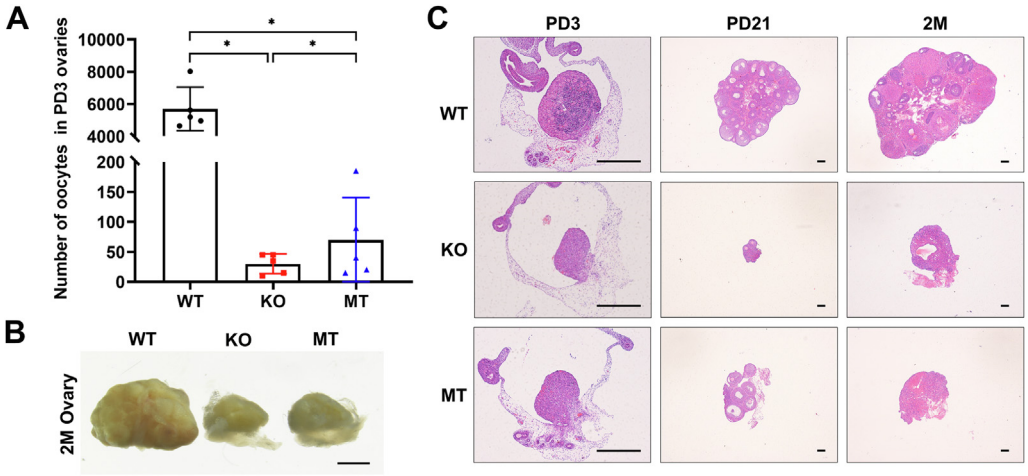

Figure 4. Oocytes in KO and MT female mice were prematurely depleted. *A*, numbers of oocytes in WT, KO, and MT ovaries at PD3. Five mice from each genotype were observed. Data are presented as mean ± SD. *$p < 0.05$. *B*, gross morphology of WT, KO, and MT ovaries at 2 months (2M). Scale bars represent 1 mm. *C*, H&E staining of WT, KO, and MT ovarian sections from PD3, PD21, and 2M mice. Scale bars represent 100 μm. KO, *Fancd2*$^{-/-}$; MT, *Fancd2*$^{K559R/K559R}$; PD, postnatal day.

KO male mice have more defects in histone methylation on meiotic sex chromosomes

Previous studies have reported that the FA core complex, FANCD2, and FANCI regulate histone methylation on XY chromosomes during meiosis (25, 29, 35). Thus, we examined the methylation of histone 3 Lysine-4 (H3K4) and histone 3 Lysine-9 (H3K9) on the meiotic XY body in KO and MT spermatocytes. While reduced accumulation of H3K4me2 on diplotene XY chromosomes was observed in KO spermatocytes, no differences in H3K4me2 on diplotene sex chromosomes were observed between WT and MT spermatocytes (Fig. 8, *A* and *B*), suggesting that FANCD2 promotes the accumulation of H3K4me2 on sex chromosomes independently of its ubiquitination. In addition, the intensity of H3K9me2 was significantly diminished (Fig. 8, *C* and *D*) and the intensity of H3K9me3 was significantly increased (Fig. 8, *E* and *F*) on diplotene XY chromosomes in both KO and MT spermatocytes. These results demonstrate that regulation of H3K9me2 and H3K9me3 on diplotene sex chromosomes is dependent on the ubiquitination of FANCD2.

KO mice display fetal growth retardation and partial embryonic lethality

The FA factors are ubiquitously expressed and growth retardation is universally observed in FA-null mice (36–38). Therefore, we compared the growth and development of the two mouse models. E9.5, E11.5, E15.5, and E18.5 embryos were collected to evaluate fetal growth by measuring the crown-rump length (Fig. S1, *A–E*). Diminished fetal lengths in both KO and MT embryos at E9.5 implied fetal growth retardation but no difference was observed between KO and MT embryos. However, from E11.5 onward, fetal lengths were decreased only in KO embryos, indicating that FANCD2 functioned in the expansion of somatic cells mainly independently of its ubiquitination. In addition, when heterozygous males and females were mated, the percentage of surviving KO pups was below the expected Mendelian ratio (Fig. S1*F*), whereas MT pups showed a close to normal Mendelian distribution (Fig. S1*G*), suggesting that the loss of FANCD2 was partially lethal. Consistent with the development delay of the KO embryos, KO pups had reduced body sizes compared with WT and MT pups. Interestingly, the differences in body weight between KO, MT, and WT adult mice both in female and male disappeared (Fig. S2, *A–D*). Congenital abnormalities are another common feature of FA-null mice, as manifested by skeletal defects, anophthalmia, opaque corneas, cranial and paw malformations, etc (36). However, both KO and MT mice appeared normal without any eye or skeletal defects in the mixed background (Fig. S2*E*). Collectively, we conclude that FANCD2 maintains the development of somatic cells independently of its ubiquitination.

Discussion

After arriving at the genital ridge, PGCs undergo rapid proliferation (31, 39). Our previous study showed that rapidly proliferating PGCs encounter high frequencies of TRCs and that the activated FA pathway protects PGCs from TRC-induced endogenous replication stress by reducing R-loop accumulation and stabilizing stalled RFs, thus ensuring the establishment of the reproductive reserve, which indicated the significant role of FANCD2 ubiquitination in PGC expansion (20). In the present study, we found that loss of PGCs in both *Fancd2* KO and MT embryos caused a significant reduction in the reproductive reserve. Furthermore, there were fewer PGCs in KO embryos than MT embryos, and more TRCs were observed in KO PGCs than in MT PGCs, implying that the ubiquitination-independent function of FANCD2 also plays a role in TRC resolution and PGC development. It has been shown that nonubiquitinated FANCD2 together with BLM and BRCA2 functions in the early response to TRCs induced by transiently blocking RNA Pol II near the promoter, and defects in this response cause increased DNA damage and cell death (12). Therefore, the defects in the early response to

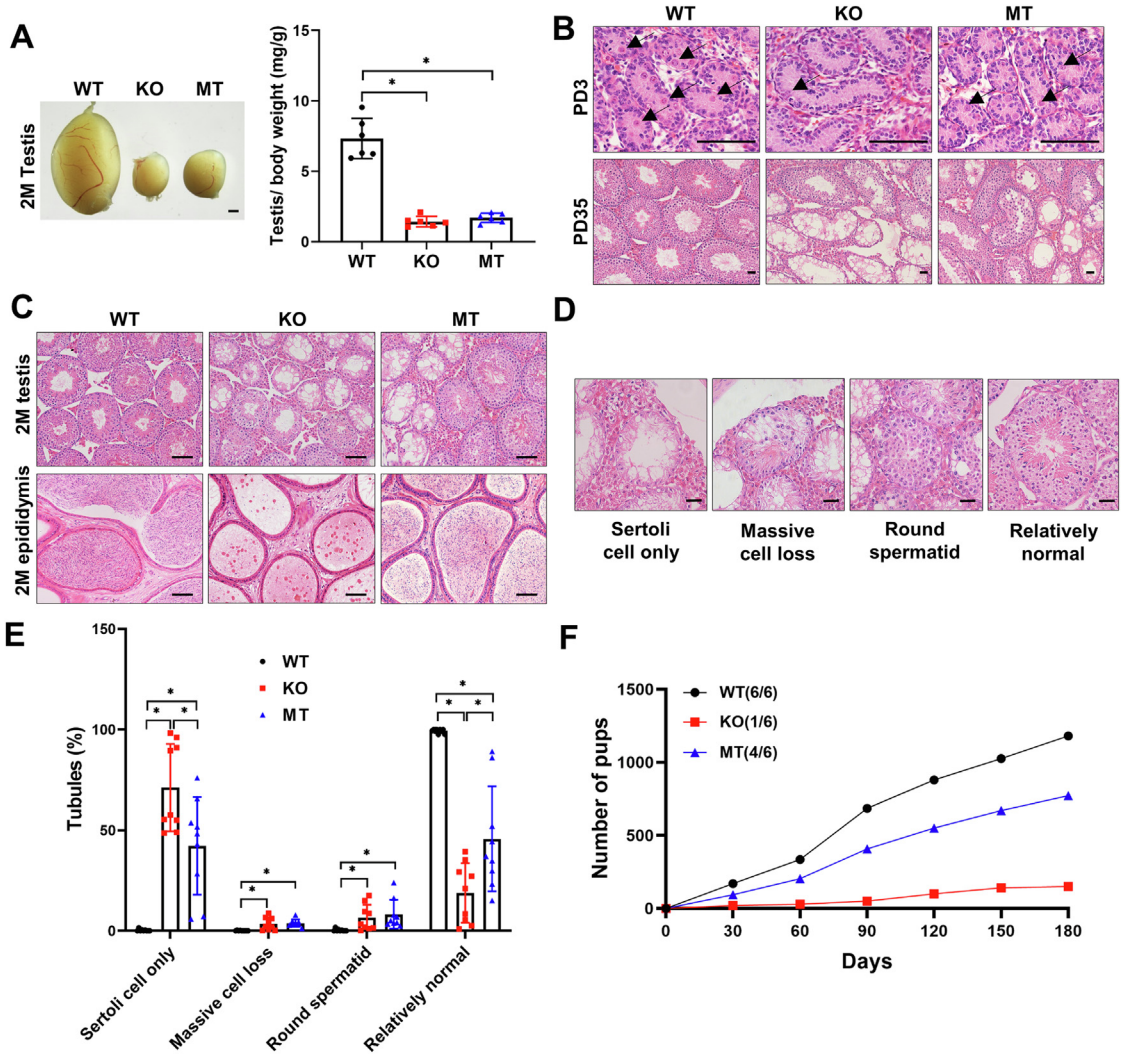

Figure 5. More germ cells were preserved in MT adult male mice compared to KO mice. *A*, gross morphology of WT, KO, and MT testes at 2M (*left*) and the testis/body weight ratio from 2M-old WT, KO, and MT mice (*right*). Scale bar represents 1 mm. Six mice from each genotype were observed. Data are presented as mean ± SD. *$p < 0.05$. *B*, H&E staining of WT, KO, and MT testes at PD3 and PD35. *Arrows* represent spermatogonia. Scale bars represent 20 μm. *C*, H&E staining of WT, KO, and MT testes and epididymides at 2M. Scale bars represent 50 μm. *D*, representative images of various types of seminiferous tubules, including tubules only with Sertoli cells, tubules with massive germ cell loss, tubules with round spermatid as the most advanced developmental stage, and tubules with relatively normal morphology. Scale bars represent 20 μm. *E*, analysis of various types of seminiferous tubules in WT, KO, and MT testes at 2M. Ten mice were included per genotype. Data are presented as mean ± SD. *$p < 0.05$. *F*, fertility test of WT, KO, and MT males. Six mice per genotype were observed. KO, *Fancd2*$^{-/-}$; MT, *Fancd2*$^{K559R/K559R}$; PD, postnatal day.

TRCs may contribute to the further increase in DNA damage and the greater reduction in PGCs in KO mice than in MT mice. In addition, under replication stress, the restarting of stalled RFs and the global suppression of new origin firing are necessary to complete DNA replication (40). Because FANCD2 also promotes stalled RF recovery and suppresses the firing of new replication origins independently of its ubiquitination (14), defects in these processes might also cause increased genome instability and further reduction of PGCs in KO embryos compared to MT embryos.

The FA pathway is well known to be involved in ICL repair and replication stress response during mitosis (41), but meiotic defects have also been reported in FA-deficient mice (15, 25, 28, 35). Male mice without FANCD2 show defects in homologous chromosome synapsis and in epigenetic modifications on XY chromosomes during meiosis (28, 29). In our study, abnormal synapsis was observed only in KO mice but not in MT mice, suggesting that FANCD2 promotes synapsis during meiosis independently of its ubiquitination. Consistent with this, no abnormalities in synapsis were observed in mice lacking FA core complex components (15, 25). Although it was previously reported that the deletion of FANCD2 had no obvious influence on HR or crossover formation in meiosis (29), abnormal γH2AX signals and increased RAD51 foci were detected in both FANCD2 KO and MT pachytene spermatocytes with a further increase in KO spermatocytes in our study, suggesting that FANCD2 functions to promote HR and DSB repair in meiosis in both a ubiquitination-dependent and ubiquitination-independent manner. During the leptotene and zygotene stages, FANCD2 foci accumulated on autosomes in a ubiquitination-dependent manner and gradually decreased at the pachytene stage, and the depletion of BRCA1 and MDC1

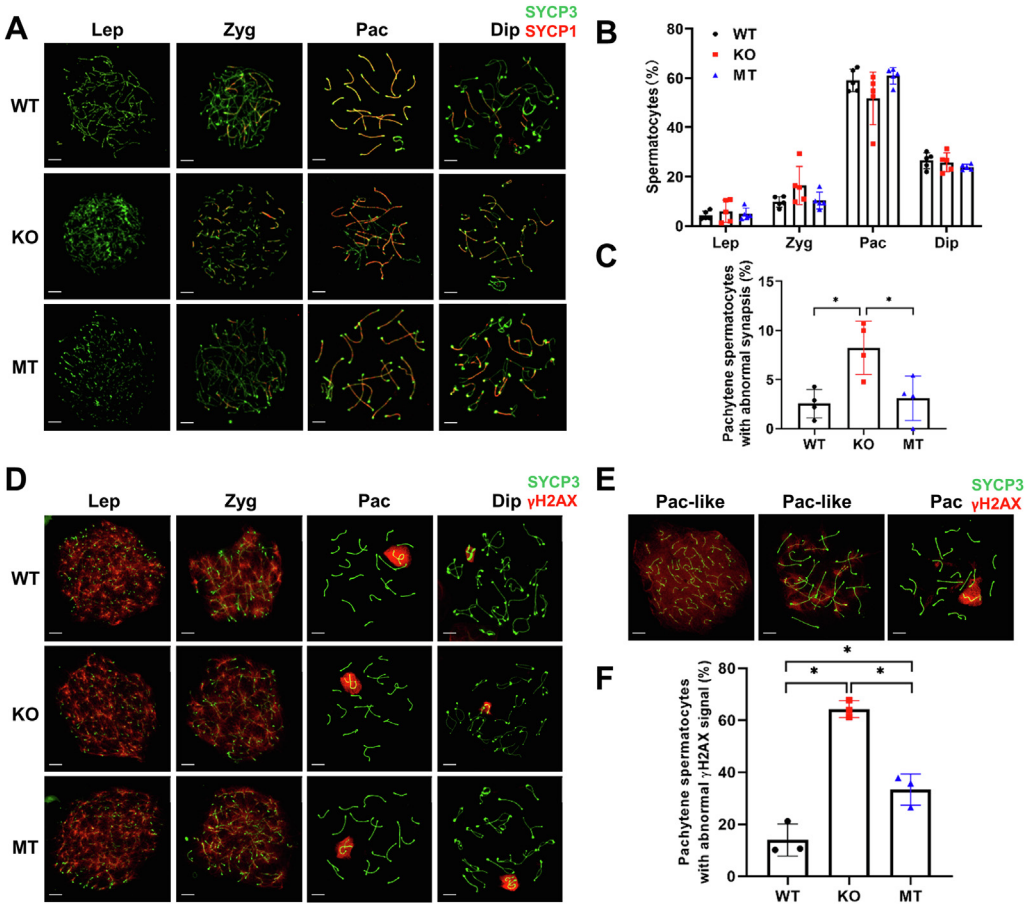

Figure 6. More defects in homologous chromosome synapsis and DSB repair were detected in KO spermatocytes. *A*, immunofluorescence staining for SYCP1 (a marker for the synaptonemal complex central region; *red*) and SYCP3 (a marker for the meiotic chromosome axis; *green*) of WT, KO, and MT spermatocyte spreads at leptotene (Lep), zygotene (Zyg), pachytene (Pac), and diplotene (Dip) stages. The meiotic stage was identified by the SYCP3 signal. Scale bars represent 5 μm. *B*, the proportion of spermatocytes in each meiotic stage in WT, KO, and MT male mice. Five mice were observed per genotype. Data are presented as mean ± SD. $*p < 0.05$. *C*, the proportion of pachytene spermatocytes with abnormal synapsis in WT, KO, and MT male mice. Four mice were analyzed per genotype. Data are presented as mean ± SD. $*p < 0.05$. *D*, immunofluorescence staining for γH2AX (*red*) and SYCP3 (*green*) in WT, KO, and MT meiotic spreads at leptotene (Lep), zygotene (Zyg), pachytene (Pac), and diplotene (Dip) stages. Scale bars represent 5 μm. *E*, representative images and *F*, the proportion of pachytene spermatocytes with abnormal γH2AX signals, including spermatocytes with γH2AX present at asynaptic sites in pachytene-like (Pac-like) cells (*left* and *middle*) and the expansion of the γH2AX domain to encompass an autosome in pachytene (Pac) cells (*right*). Scale bars represent 5 μm. Data are presented as mean ± SD. $*p < 0.05$. γH2AX, phosphorylated H2AX; DSB, double strand breaks; KO, *Fancd2*$^{-/-}$; MT, *Fancd2*$^{K559R/K559R}$.

increased the number of FANCD2 foci on autosomes at the pachytene stage (29), suggesting that the localization of FANCD2 on autosomes may represent the DSB sites. While the FANCD2 homolog fcd-2 is required for HR during meiotic DSB repair in *Caenorhabditis elegans* (42), FANCD2 also promotes DSB repair through HR independently of its ubiquitination in human somatic cells (13, 43). However, the function and mechanism of FANCD2 in mammalian meiotic DSB repair needs further investigation. Although increased γH2AX signals were observed in KO and MT pachytene spermatocytes, the progression of meiosis was not arrested. Furthermore, a small subset of KO and MT diplotene spermatocytes still contained abnormally increased γH2AX signals on autosomes, indicating that the number of unrepaired DSBs was below the threshold for causing meiosis arrest. In addition, we also observed increased crossover formation in KO spermatocytes. Both the unrepaired DSBs and increased crossovers may cause genome instability in spermatocytes, thus leading to the almost complete absence of sperm in KO mice.

During male meiosis, the X and Y chromosomes are transcriptionally silenced, which is known as meiotic sex chromosome inactivation (44). DDR factors, such as H2AX, BRCA1, and MDC1, play an important role in meiotic sex chromosome inactivation initiation (45–47). As DDR factors accumulate, epigenetic modifiers are recruited and histone modifications are established on sex chromosomes during meiosis, and these regulate transcription of the XY chromosomes over the course of meiosis and into postmeiotic stages (48, 49). Recently, it was reported that FA core complex proteins (FANCA, FANCB, and FANCC) and FANCD2 regulated the epigenetic modification of XY chromosomes in meiosis (25, 29), and our previous study showed that FANCI also functions in this process (35). In this study, we further demonstrated that in diplotene spermatocytes, FANCD2 upregulated H3K9me2 and suppressed H3K9me3 on XY chromosomes in a ubiquitination-dependent manner, whereas the accumulation of H3K4me2 on XY chromosomes was independent of FANCD2 ubiquitination. Consistent with this, it

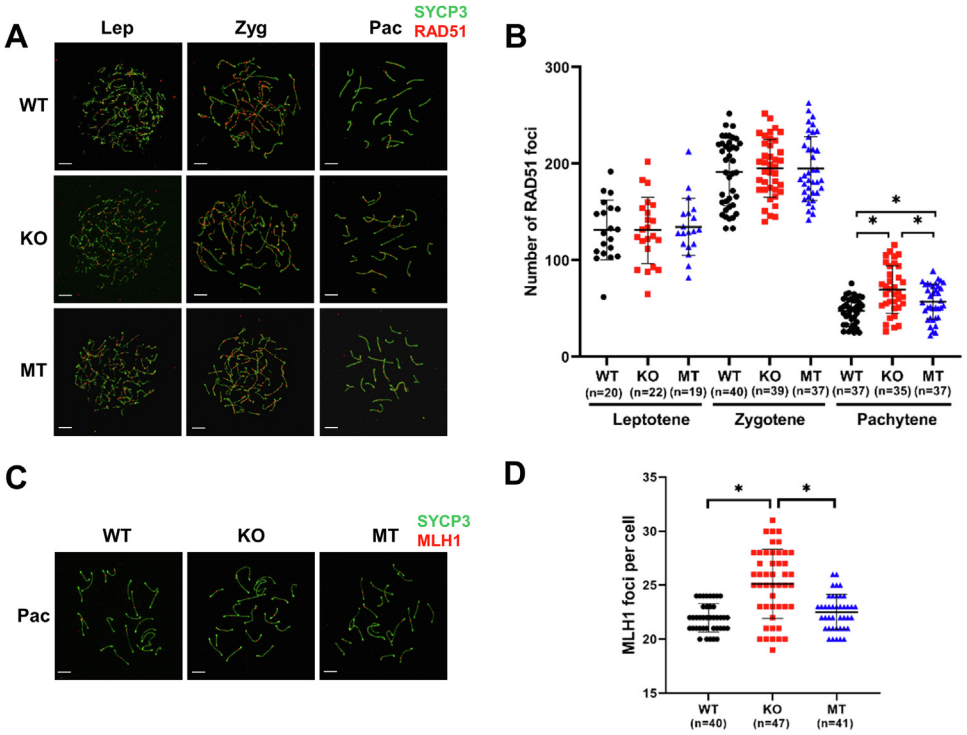

Figure 7. Homologous recombination defects and increased crossover formation were observed in KO spermatocytes. *A*, immunofluorescence staining for RAD51 (a marker for meiotic recombination event, *red*) and SYCP3 (*green*) of WT, KO, and MT spermatocyte spreads at leptotene (Lep), zygotene (Zyg), pachytene (Pac) stages. Scale bars represent 5 μm. *B*, the number of RAD51 foci in leptotene, zygotene, and pachytene spermatocytes in WT, KO, and MT male mice. Data are presented as mean ± SD. *$p < 0.05$. *C*, immunofluorescence staining for MLH1 (a marker for potential crossover, *red*) and SYCP3 (*green*) of WT, KO, and MT spermatocyte spreads at pachytene (Pac) stage. Scale bars represent 5 μm. *D*, the number of MLH1 foci in pachytene spermatocytes in WT, KO, and MT male mice. Data are presented as mean ± SD. *$p < 0.05$. KO, *Fancd2*$^{-/-}$; MT, *Fancd2*$^{K559R/K559R}$.

was previously reported that FANCD2 functions downstream of RNF8 to upregulate H3K4me2 on sex chromosomes (29) and that RNF8-dependent H3K4me2 accumulation activates the expression of reproduction-related genes in round spermatids (50). Some of these genes, such as the *Ssty* gene family and *Ar*, are crucial for the maturation of spermatozoa and for the normal function of sperm (51, 52). Thus, although no obvious changes in global transcription level were observed in *Fancd2* KO spermatocytes (29), the reduction of H3K4me2 on sex chromosomes in KO males might affect the transcription of these reproduction-related genes and further aggravate sperm abnormalities. Furthermore, the lysine methyltransferase SETD1A catalyzes H3K4 methylation at stalled RFs to prevent the nucleolytic degradation of RFs during mitosis, and this activity is dependent on histone chaperone activity but is independent of the ubiquitination of FANCD2 (53). Whether FANCD2 regulates histone methylation on sex chromosomes during meiosis through a similar mechanism needs to be determined.

Similar to the phenotypes of *Fancd2* KO and MT mice, increased γH2AX signals and RAD51 foci in pachytene spermatocytes were observed in mice deficient in CXXC1, NAT10, or CNOT4, suggesting that CXXC1-regulated H3K4me3 accumulation, CNOT4-mediated mRNA degradation, and NAT10-dependent RNA ac4C modification also affect meiotic DSB repair and genome stability during male germ cell development (54–56). Although we have determined the ubiquitination-dependent and ubiquitination-independent functions of FANCD2 in regulating histone methylation on meiotic sex chromosomes, the potential relationship between FANCD2 and the above epigenetic or mRNA regulators in maintaining genome stability during spermatogenesis remains to be determined.

In our study, the KO mice with mixed background had similar phenotypes as those reported by Houghtaling *et al.*, such as hypogonadism, partial embryonic lethality, and developmental retardation (28), but they manifested milder phenotypes than those reported by Nie *et al.* and Yang *et al.* in which KO mice in the C57BL/6J background displayed more severe hypogonadism with complete loss of germ cells in the testes, higher rates of embryonic lethality, and higher incidence of microphthalmia (27, 37). Phenotypic differences may be related to the distinct genetic background of the mice. While oocytes were unable to regenerate and the few remaining follicles were rapidly exhausted in KO and MT females, the spermatogonia derived from the remaining PGCs could persistently proliferate and differentiate into spermatogenic cells in their male counterparts. Together, both more remaining PGCs and fewer meiotic defects might account for the recovery of fertility in more than half of the MT male mice.

In summary, we identified distinct functions of FANCD2 that are either dependent on or independent of ubiquitination in germ cell development, and the rapid proliferation and TRC

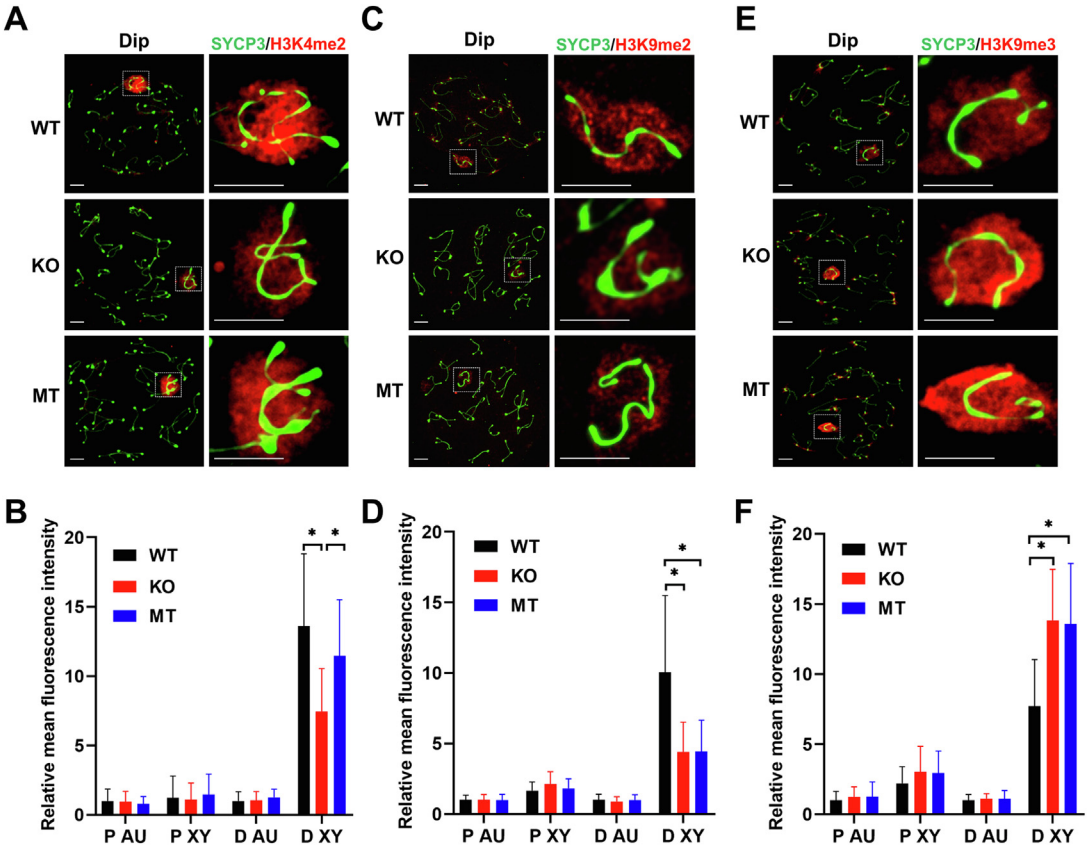

Figure 8. KO male mice showed more defects in histone methylation on meiotic sex chromosomes. Immunofluorescence staining for SYCP3 (*green*) and H3K4me2 (*red*) (*A*), H3K9me2 (*red*) (*C*), and H3K9me3 (*red*) (*E*) in WT, KO, and MT diplotene (Dip) spermatocytes. Scale bars represent 5 μm. Analysis of the relative mean fluorescence intensity of H3K4me2 (*B*), H3K9me2 (*D*), and H3K9me3 (*F*) on autosome regions (AU) and XY chromosomes in WT, KO, and MT pachytene (P) and diplotene (D) spermatocytes. A total of 40 cells were included each group. Data are presented as mean ± SD. *$p < 0.05$. H3K4, histone 3 Lysine-4; H3K9, histone 3 Lysine-9; KO, *Fancd2*$^{-/-}$; MT, *Fancd2*$^{K559R/K559R}$.

resolution in PGCs required both the ubiquitination-dependent and ubiquitination-independent functions of FANCD2. Furthermore, meiotic progress during spermatogenesis required both ubiquitinated and nonubiquitinated FANCD2, and the regulation of H3K4 and H3K9 methylation on meiotic XY chromosomes required its nonubiquitinated and ubiquitinated functions, respectively. Our findings provide deeper insights into the roles of FANCD2 in gametogenesis and help to reveal the pathogenesis of FA-related reproductive defects.

Experimental procedures

Generation of the KO and MT mouse models

Both KO and MT mice were generated by Cyagen Biosciences Company using CRISPR/Cas9 technology. For KO mice, the gRNAs (gRNA1: GGC GAA AAA TAT TCT TAG TAG GG, gRNA2: GGT GGT TAG ATG ACA TTG AAG GG) for the *Fancd2* gene and Cas9 mRNA were mixed and injected into the cytoplasm of fertilized eggs to generate targeted KO mice. For MT mice, the gRNA (CAG TGC TAG AGA GCT GCT TCC GG) to the mouse *Fancd2* gene, the donor oligo containing p.K559R (AAG to AGG) missense mutation and p.R558= (CGG to CGA) synonymous mutation, and Cas9 mRNA were mixed and injected into the cytoplasm of fertilized eggs to generate MT mice (20). F0 founder mice were identified by PCR and bred with WT mice to acquire F1 heterozygous animals. Heterozygous mice were intercrossed to generate homozygous mice. Mice with a C57BL/6J × ICR–mixed genetic background were used in this study. Our study procedures were conducted in accordance with the ethical guidelines approved by the animal care and research committee of Shandong University.

Genotyping

Mouse tail tips were digested for 15 min at 95 °C in 100 μl solution A (25 mM NaOH), then mixed in Eppendorf tubes with equal volumes of solution B (40 mM Tris–HCl) for neutralization. After mixing the solution and centrifuging for 10 min at 400*g*, the supernatant containing fragments of mouse genomic DNA was obtained. PCR reactions were performed in 20 μl volumes, including 1 μl DNA extract, 0.1 μl Takara Ex Taq HS, 2 μl 10 × Ex Taq Buffer, 1.6 μl dNTP mixture, 0.5 μl forward primer, 0.5 μl reverse primer, and 14.3 μl ddH_2O. The PCR primers were as follows: *Fancd2*-KO-F1 (TAC CCA GGA AGC AAG TAG ATC TGT A), *Fancd2*-KO-R1 (TAA AGC AAC TAT CAG CTC TCA CAG) and R2 (ACA TCT GAT GAC GCC ACT AAG AAT A), *Fancd2*-MT-F1 (ATT CCA CAG TGA TTC TCA AGT CCT), and *Fancd2*-MT-R1 (GAT CTC CCA AGT TGC AAA GTA GAC).

Primary MEF cell culture and Western blotting

For isolating primary MEF cells, WT, KO, and MT embryos at E13.5 were collected in PBS with 2% penicillin-streptomycin and the head, limbs, and viscera were removed. Each embryo was cut into pieces and then suspended and digested in 1 ml 0.05% trypsin at 37 °C for 4 min. The digestion was terminated by adding 2 ml of Dulbecco's modified Eagle medium (Gibco) containing 10% fetal calf serum (Gibco). Each suspension was centrifuged at 200*g* for 5 min. After discarding the supernatant, cells were resuspended and cultured in Dulbecco's modified Eagle medium containing 10% fetal calf serum. To examine the activation of the FA pathway, MEFs were exposed to 50 ng/ml MMC for 24 h before protein extraction.

For Western blotting, cells were lysed with SDS supplemented with proteinase inhibitor, and then the lysates were boiled at 100 °C for 8 min. The samples containing 20 μg of protein were subjected to SDS-PAGE and then transferred onto polyvinylidene fluoride membrane (Millipore Corporation). After blocked in 5% milk for 1 h at room temperature (RT), the membrane was incubated with the FANCD2 antibody (ab108928, 1:1000 dilution) overnight at 4 °C. Then, the membrane was washed in tris buffered saline with Tween-20 (20 mM Tris–HCl, PH 7.6, 137 mM NaCl, and 0.1% Tween 20) three times and was incubated with the corresponding secondary antibody (Proteintech) for 1 h at RT. The signal was detected with an ECL system (Millipore), and images were acquired using the ChemiDoc MP System (Bio-Rad).

Alkaline phosphatase staining, immunofluorescence, H&E staining

For alkaline phosphatase staining, fixed embryos at E8.5, E9.5, and E11.5 were washed with Tris–Maleate buffer (25 mM, PH 9.0) for 10 min two times. Alkaline phosphatase staining was performed in the dark place in 25 ml Tris–Maleate buffer (25 mM, PH 9.0), 125 μl 100 mM $MgCl_2$, 10 mg 1-Naphthyl phosphate, disodium salt, and 25 mg Fast Red TR salt (Sigma). The staining reaction was protected from light and processed for 15 min at 37 °C, and the reaction was terminated by adding PBS. After washing with PBS two times, the organs were made transparent by soaking in 40% glycerinum for 1 h and 80% glycerinum overnight at 4 °C. Imaging was performed on stereoscope (Nikon).

For immunofluorescence staining, genital ridges at E11.5, ovaries and testes at E13.5 and E18.5 were cut into 10 μm frozen sections. After blocking with 25% donkey serum plus 0.3% Triton X-100 for 1 h at RT, the sections were incubated with primary antibodies in 10% BSA plus 0.1% Triton X-100 overnight at 4 °C. Following washing in PBS plus 0.01% Triton X-100 (0.01% PBST), the sections were incubated with corresponding secondary antibodies and Hoechst 33342 (Yeasen 40731ES10, 1:800) in PBS plus 0.1% Triton X-100 for 1 h at RT. Next, the sections were washed and mounted with Antifade Medium (Invitrogen). The following primary antibodies were used: rabbit anti-FANCD2 (Abcam ab108928, 1:300 dilution), goat anti-STELLA (Novus biologicals AF2566, 1:50 dilution), goat anti-DDX4 (Novus AF2030, 1:50 dilution), rabbit anti-FOXL2 (Abcam ab246511, 1:250 dilution), rabbit anti-SOX9 (Millipore AB5535, 1:200 dilution), mouse anti-proliferating cell nuclear antigen (Santa Cruz SC-56, 1:25 dilution), rabbit anti-Pol II (Abcam ab26721, 1:100 dilution), rabbit anti-53BP1 (Novus NB100-304, 1:500 dilution), rabbit anti-SYCP1 (Abcam ab15090, 1:500 dilution), rabbit anti-SYCP3 (Abcam ab15093, 1:500 dilution), mouse anti-SYCP3 (Abcam ab97672, 1:500 dilution), mouse anti-γH2AX (Millipore 05-636, 1:500 dilution), rabbit anti-RAD51 (Invitrogen PA5-27195, 1:100 dilution), mouse anti-MLH1 (BD Biosciences 550838, 1:50 dilution), rabbit anti-H3K4me2 (Millipore 07-030, 1:200 dilution), rabbit anti-H3K9me2 (Millipore 07-44,1 1:500 dilution), and rabbit anti-H3K9me3 (Millipore 07-442, 1:500 dilution). fluorescein isothiocyanate and tetramethyl rhodamine isothiocyanate-conjugated secondary antibodies (Invitrogen) were used. Images were acquired by Dragonfly spinning disc confocal microscope (ANDOR Technology).

For H&E staining, ovaries and testes were fixed in 4% paraformaldehyde or Bouin's solution overnight at 4 °C and were dehydrated and embedded in paraffin. Ovaries and testes were sectioned at 5 μm and stained with H&E. Histological images were acquired using an Olympus BX53 microscope.

Proximity ligation assay

E11.5 genital ridges from WT, KO, and MT embryos were collected to perform PLA as previously described (20). Briefly, after incubated with primary antibodies, the sections were incubated with probes (Duolink *in situ* PLA probes anti-mouse plus and anti-rabbit minus diluted 1:5) for 1 h at 37 °C. Then, sections were washed with buffer A and incubated in ligation mix (Duolink ligation stock and ligase diluted 1:5 and 1:40, respectively) for 30 min at 37 °C. After that, the sections were washed with buffer A and incubated in amplification mix (Duolink amplification stock and polymerase diluted 1:5 and 1:80, respectively) for 100 min at 37 °C. In order to indicate PGCs, immunofluorescence staining for STELLA antibody was performed after PLA.

Fertility test

Six WT, KO, and MT male mice aged 8 weeks were selected, and each male mouse was singly housed with two WT female mice aged 8 weeks. The number of offspring from the female mice over 6 months was recorded continuously, and pups were counted on the first day of life.

Meiotic chromosome spreads

WT, KO, and MT male mice were selected to prepare meiotic chromosome spreads as previously described (29). In brief, testicular tubules were incubated with hypotonic extraction buffer for 40 min at RT and then minced into a single-cell suspension in 100 mM sucrose solution. The cell suspension was spread onto slides coated with the fixation solution (1% paraformaldehyde and 0.1% Triton X-100), and the slides were maintained in a humidified chamber overnight at 4 °C prior to immunofluorescence staining.

The quantification of the relative mean fluorescence intensity of histone methylation was performed by ImageJ software (https://imagej.net/). We normalized the regions of interest of sex chromosomes and autosomes to the background signal. The relative mean fluorescence intensities in both pachytene and diplotene spermatocytes were analyzed in this study.

Statistical analysis

All analyses were conducted in Prism 8 (GraphPad Software). Unpaired two-tailed Student's t tests were used to compare differences between groups, and value of $p < 0.05$ was considered statistically significant.

Data availability

All data are available in the main article or the supporting information.

Supporting information—This article contains supporting information.

Acknowledgments—This work was supported by grants from the National Key Research and Development Program of China (2021YFC2700100 and 2022YFC2703800), National Natural Science Foundation of China (32170867, 81873823, and 32070847), Basic Science Center Program of National Natural Science Foundation of China (31988101), Natural Science Foundation of Shandong Province for Grand Basic Projects (ZR2021ZD33), Shandong Provincial Key Research and Development Program (2020ZLYS02), Research Unit of Gametogenesis and Health of ART-Offspring, Chinese Academy of Medical Sciences (2020RU001), Taishan Scholars Program for Young Experts of Shandong Province, Qilu Young Scholars Program of Shandong University, and Innovative research team of high-level local universities in Shanghai (SHSMU-ZLCX20210200).

Author contributions—Si. Z. and C. H. investigation; Si. Z., C. H., W. X., Yo. Y., C. W., and L. C. formal analysis; Si. Z. writing-original draft; Ya. Y., Y. Q., Z.-J. C., T. G., and Sh. Z. methodology; Ya. Y., F. G., and Sh. Z. writing-review & editing.

Conflict of interest—The authors declare that they have no conflicts of interest with the contents of this article.

Abbreviations—The abbreviations used are: DDR, DNA damage response; DSB, double strand break; FA, Fanconi anemia; H3K4, histone 3 Lysine 4; H3K9, histone 3 Lysine 9; HR, homologous recombination; ICL, interstrand crosslink; KO, *Fancd2*$^{-/-}$; MEF, mouse embryonic fibroblast; MMC, mitomycin C; MT, *Fancd2*$^{K559R/K559R}$; PD, postnatal day; PGC, primordial germ cell; PFA, paraformaldehyde; PLA, proximity ligation assay; Pol II, RNA polymerase II; RF, replication fork; RT, room temperature; TRC, transcription-replication conflict; γH2AX, phosphorylated H2AX.

References

1. Saitou, M., Kagiwada, S., and Kurimoto, K. (2012) Epigenetic reprogramming in mouse pre-implantation development and primordial germ cells. *Development (Cambridge, England)* **139**, 15–31
2. Bolcun-Filas, E., and Handel, M. A. (2018) Meiosis: the chromosomal foundation of reproduction. *Biol. Reprod.* **99**, 112–126
3. Joenje, H., and Patel, K. J. (2001) The emerging genetic and molecular basis of Fanconi anaemia. *Nat. Rev. Genet.* **2**, 446–457
4. Kottemann, M. C., and Smogorzewska, A. (2013) Fanconi anaemia and the repair of Watson and Crick DNA crosslinks. *Nature* **493**, 356–363
5. Semlow, D. R., and Walter, J. C. (2021) Mechanisms of Vertebrate DNA interstrand cross-link repair. *Annu. Rev. Biochem.* **90**, 107–135
6. Nalepa, G., and Clapp, D. W. (2018) Fanconi anaemia and cancer: an intricate relationship. *Nat. Rev. Cancer* **18**, 168–185
7. Taniguchi, T., Garcia-Higuera, I., Andreassen, P. R., Gregory, R. C., Grompe, M., and D'Andrea, A. D. (2002) S-phase-specific interaction of the Fanconi anemia protein, FANCD2, with BRCA1 and RAD51. *Blood* **100**, 2414–2420
8. Alpi, A. F., and Patel, K. J. (2009) Monoubiquitylation in the Fanconi anemia DNA damage response pathway. *DNA repair* **8**, 430–435
9. García-Muse, T., and Aguilera, A. (2016) Transcription-replication conflicts: How they occur and how they are resolved. *Nat. Rev. Mol. Cell Biol.* **17**, 553–563
10. Gómez-González, B., and Aguilera, A. (2019) Transcription-mediated replication hindrance: a major driver of genome instability. *Genes Dev.* **33**, 1008–1026
11. Tian, Y., Shen, X., Wang, R., Klages-Mundt, N. L., Lynn, E. J., Martin, S. K., *et al.* (2017) Constitutive role of the Fanconi anemia D2 gene in the replication stress response. *J. Biol. Chem.* **292**, 20184–20195
12. Shao, X., Joergensen, A. M., Howlett, N. G., Lisby, M., and Oestergaard, V. H. (2020) A distinct role for recombination repair factors in an early cellular response to transcription-replication conflicts. *Nucl. Acids Res.* **48**, 5467–5484
13. Kachnic, L. A., Li, L., Fournier, L., Ferraiolo, N., Dahm-Daphi, J., Borgmann, K., *et al.* (2011) FANCD2 but not FANCA promotes cellular resistance to type II topoisomerase poisons. *Cancer Lett.* **305**, 86–93
14. Raghunandan, M., Chaudhury, I., Kelich, S. L., Hanenberg, H., and Sobeck, A. (2015) FANCD2, FANCJ and BRCA2 cooperate to promote replication fork recovery independently of the Fanconi Anemia core complex. *Cell Cycle (Georgetown, Tex.)* **14**, 342–353
15. Wong, J. C., Alon, N., McKerlie, C., Huang, J. R., Meyn, M. S., and Buchwald, M. (2003) Targeted disruption of exons 1 to 6 of the Fanconi Anemia group A gene leads to growth retardation, strain-specific microphthalmia, meiotic defects and primordial germ cell hypoplasia. *Hum. Mol. Genet.* **12**, 2063–2076
16. Fouquet, B., Pawlikowska, P., Caburet, S., Guigon, C., Mäkinen, M., Tanner, L., *et al.* (2017) A homozygous FANCM mutation underlies a familial case of non-syndromic primary ovarian insufficiency. *eLife* **6**, e30490
17. Fu, C., Begum, K., and Overbeek, P. A. (2016) Primary ovarian insufficiency induced by Fanconi anemia E mutation in a mouse model. *PLoS One* **11**, e0144285
18. Yang, Y., Guo, J., Dai, L., Zhu, Y., Hu, H., Tan, L., *et al.* (2018) XRCC2 mutation causes meiotic arrest, azoospermia and infertility. *J. Med. Genet.* **55**, 628–636
19. Knies, K., Inano, S., Ramírez, M. J., Ishiai, M., Surrallés, J., Takata, M., *et al.* (2017) Biallelic mutations in the ubiquitin ligase RFWD3 cause Fanconi anemia. *J. Clin. Invest.* **127**, 3013–3027
20. Yang, Y., Xu, W., Gao, F., Wen, C., Zhao, S., Yu, Y., *et al.* (2022) Transcription-replication conflicts in primordial germ cells necessitate the Fanconi anemia pathway to safeguard genome stability. *Proc. Natl. Acad. Sci. U. S. A.* **119**, e2203208119
21. Tsui, V., and Crismani, W. (2019) The Fanconi anemia pathway and fertility. *Trends Genet.* **35**, 199–214
22. Simhadri, S., Peterson, S., Patel, D. S., Huo, Y., Cai, H., Bowman-Colin, C., *et al.* (2014) Male fertility defect associated with disrupted BRCA1-PALB2 interaction in mice. *J. Biol. Chem.* **289**, 24617–24629
23. Sun, X., Brieño-Enríquez, M. A., Cornelius, A., Modzelewski, A. J., Maley, T. T., Campbell-Peterson, K. M., *et al.* (2016) FancJ (Brip1) loss-of-function allele results in spermatogonial cell depletion during embryogenesis and altered processing of crossover sites during meiotic prophase I in mice. *Chromosoma* **125**, 237–252
24. Kuznetsov, S., Pellegrini, M., Shuda, K., Fernandez-Capetillo, O., Liu, Y., Martin, B. K., *et al.* (2007) RAD51C deficiency in mice results in early

prophase I arrest in males and sister chromatid separation at metaphase II in females. *J. Cell Biol.* **176**, 581–592
25. Kato, Y., Alavattam, K. G., Sin, H. S., Meetei, A. R., Pang, Q., Andreassen, P. R., *et al.* (2015) FANCB is essential in the male germline and regulates H3K9 methylation on the sex chromosomes during meiosis. *Hum. Mol. Genet.* **24**, 5234–5249
26. Yin, H., Ma, H., Hussain, S., Zhang, H., Xie, X., Jiang, L., *et al.* (2019) A homozygous FANCM frameshift pathogenic variant causes male infertility. *Genet. Med.* **21**, 62–70
27. Nie, Y., Wilson, A. F., DeFalco, T., Meetei, A. R., Namekawa, S. H., and Pang, Q. (2020) FANCD2 is required for the repression of germline transposable elements. *Reproduction (Cambridge, England)* **159**, 659–668
28. Houghtaling, S., Timmers, C., Noll, M., Finegold, M. J., Jones, S. N., Meyn, M. S., *et al.* (2003) Epithelial cancer in Fanconi anemia complementation group D2 (Fancd2) knockout mice. *Genes Dev.* **17**, 2021–2035
29. Alavattam, K. G., Kato, Y., Sin, H. S., Maezawa, S., Kowalski, I. J., Zhang, F., *et al.* (2016) Elucidation of the Fanconi anemia protein network in meiosis and its function in the regulation of histone modifications. *Cell Rep.* **17**, 1141–1157
30. Percharde, M., Wong, P., and Ramalho-Santos, M. (2017) Global hypertranscription in the mouse embryonic germline. *Cell Rep.* **19**, 1987–1996
31. Kagiwada, S., Kurimoto, K., Hirota, T., Yamaji, M., and Saitou, M. (2013) Replication-coupled passive DNA demethylation for the erasure of genome imprints in mice. *EMBO J.* **32**, 340–353
32. Murina, O., von Aesch, C., Karakus, U., Ferretti, L. P., Bolck, H. A., Hänggi, K., *et al.* (2014) FANCD2 and CtIP cooperate to repair DNA interstrand crosslinks. *Cell Rep.* **7**, 1030–1038
33. Ceccaldi, R., Sarangi, P., and D'Andrea, A. D. (2016) The Fanconi anaemia pathway: new players and new functions. *Nat. Rev. Mol. Cell Biol.* **17**, 337–349
34. Gray, S., and Cohen, P. E. (2016) Control of meiotic crossovers: from double-strand break formation to designation. *Annu. Rev. Genet.* **50**, 175–210
35. Xu, L., Xu, W., Li, D., Yu, X., Gao, F., Qin, Y., *et al.* (2021) FANCI plays an essential role in spermatogenesis and regulates meiotic histone methylation. *Cell Death Dis.* **12**, 780
36. Dubois, E. L., Guitton-Sert, L., Béliveau, M., Parmar, K., Chagraoui, J., Vignard, J., *et al.* (2019) A Fanci knockout mouse model reveals common and distinct functions for FANCI and FANCD2. *Nucl. Acids Res.* **47**, 7532–7547
37. Yang, Q., Xie, H., Zhong, Y., Li, D., Ke, X., Ying, H., *et al.* (2019) Severe Fanconi anemia phenotypes in Fancd2 depletion mice. *Biochem. Biophys. Res. Commun.* **514**, 713–719
38. Kim, J. M., Parmar, K., Huang, M., Weinstock, D. M., Ruit, C. A., Kutok, J. L., *et al.* (2009) Inactivation of murine Usp1 results in genomic instability and a Fanconi anemia phenotype. *Dev. Cell* **16**, 314–320
39. Seki, Y., Yamaji, M., Yabuta, Y., Sano, M., Shigeta, M., Matsui, Y., *et al.* (2007) Cellular dynamics associated with the genome-wide epigenetic reprogramming in migrating primordial germ cells in mice. *Development (Cambridge, England)* **134**, 2627–2638
40. Saldivar, J. C., Cortez, D., and Cimprich, K. A. (2017) The essential kinase ATR: Ensuring faithful duplication of a challenging genome. *Nat. Rev. Mol. Cell Biol.* **18**, 622–636
41. Lopez-Martinez, D., Liang, C. C., and Cohn, M. A. (2016) Cellular response to DNA interstrand crosslinks: the Fanconi anemia pathway. *Cell Mol. Life Sci.* **73**, 3097–3114
42. Adamo, A., Collis, S. J., Adelman, C. A., Silva, N., Horejsi, Z., Ward, J. D., *et al.* (2010) Preventing nonhomologous end joining suppresses DNA repair defects of Fanconi anemia. *Mol. Cel.* **39**, 25–35
43. Pace, P., Mosedale, G., Hodskinson, M. R., Rosado, I. V., Sivasubramaniam, M., and Patel, K. J. (2010) Ku70 corrupts DNA repair in the absence of the Fanconi anemia pathway. *Science (New York, N.Y.)* **329**, 219–223
44. Turner, J. M. (2007) Meiotic sex chromosome inactivation. Development (Cambridge, England) **134**, 1823–1831
45. Broering, T. J., Alavattam, K. G., Sadreyev, R. I., Ichijima, Y., Kato, Y., Hasegawa, K., *et al.* (2014) BRCA1 establishes DNA damage signaling and pericentric heterochromatin of the X chromosome in male meiosis. *J. Cell Biol.* **205**, 663–675
46. Fernandez-Capetillo, O., Mahadevaiah, S. K., Celeste, A., Romanienko, P. J., Camerini-Otero, R. D., Bonner, W. M., *et al.* (2003) H2AX is required for chromatin remodeling and inactivation of sex chromosomes in male mouse meiosis. *Dev. Cell* **4**, 497–508
47. Ichijima, Y., Ichijima, M., Lou, Z., Nussenzweig, A., Camerini-Otero, R. D., Chen, J., *et al.* (2011) MDC1 directs chromosome-wide silencing of the sex chromosomes in male germ cells. *Genes Dev.* **25**, 959–971
48. van der Heijden, G. W., Derijck, A. A., Pósfai, E., Giele, M., Pelczar, P., Ramos, L., *et al.* (2007) Chromosome-wide nucleosome replacement and H3.3 incorporation during mammalian meiotic sex chromosome inactivation. *Nat. Genet.* **39**, 251–258
49. Kimmins, S., and Sassone-Corsi, P. (2005) Chromatin remodelling and epigenetic features of germ cells. *Nature* **434**, 583–589
50. Sin, H. S., Barski, A., Zhang, F., Kartashov, A. V., Nussenzweig, A., Chen, J., *et al.* (2012) RNF8 regulates active epigenetic modifications and escape gene activation from inactive sex chromosomes in post-meiotic spermatids. *Genes Dev.* **26**, 2737–2748
51. Touré, A., Clemente, E. J., Ellis, P., Mahadevaiah, S. K., Ojarikre, O. A., Ball, P. A., *et al.* (2005) Identification of novel Y chromosome encoded transcripts by testis transcriptome analysis of mice with deletions of the Y chromosome long arm. *Genome Biol.* **6**, R102
52. O'Hara, L., Welsh, M., Saunders, P. T., and Smith, L. B. (2011) Androgen receptor expression in the caput epididymal epithelium is essential for development of the initial segment and epididymal spermatozoa transit. *Endocrinology* **152**, 718–729
53. Higgs, M. R., Sato, K., Reynolds, J. J., Begum, S., Bayley, R., Goula, A., *et al.* (2018) Histone methylation by SETD1A protects nascent DNA through the nucleosome chaperone activity of FANCD2. *Mol. Cell* **71**, 25–41.e26
54. Dai, X. X., Jiang, Y., Gu, J. H., Jiang, Z. Y., Wu, Y. W., Yu, C., *et al.* (2021) The CNOT4 subunit of the CCR4-NOT complex is involved in mRNA degradation, efficient DNA damage repair, and XY chromosome crossover during male germ cell meiosis. *Adv. Sci. (Weinheim, Baden-Wurttemberg, Germany)* **8**, 2003636
55. Chen, L., Wang, W. J., Liu, Q., Wu, Y. K., Wu, Y. W., Jiang, Y., *et al.* (2022) NAT10-mediated N4-acetylcytidine modification is required for meiosis entry and progression in male germ cells. *Nucl. Acids Res.* **50**, 10896–10913
56. Jiang, Y., Zhang, H. Y., Lin, Z., Zhu, Y. Z., Yu, C., Sha, Q. Q., *et al.* (2020) CXXC finger protein 1-mediated histone H3 lysine-4 trimethylation is essential for proper meiotic crossover formation in mice. *Development (Cambridge, England)* **147**, dev183764